Empirical evidence of a superrigid structure of "flat" superdeformed bands

Anshul Dadwal* and H. M. Mittal
Dr. B. R. Ambedkar National Institute of Technology, Jalandhar 144011, India

(Received 13 August 2018; published 10 April 2019)

For the first time, we present the empirical evidence of superrigid character of the "flat" superdeformed bands in the Tl and Pb isotopes. For this purpose, we have used various rotational energy formulas. The free parameters of superdeformed (SD) bands in the Tl and Pb isotopes have been extracted and systematically studied to obtain the proposed empirical evidence. In particular, the intraband transition energies of the SD bands have been split into rotational and shape fluctuation energies. The role of the vibrational factor in the evolution of dynamic moment of inertia, softness parameter, alignment, and effective pairing gap parameter of the flat SD bands has been studied. Using these models, two distinct natures have been identified for the SD bands in the Tl and Pb isotopes. Our study establishes the role of shape fluctuations, vibrational effect, deformation, and pairing correlations for the unusual behavior of the dynamic moment of inertia in the flat SD bands of the $A \approx 190$ mass region.

DOI: 10.1103/PhysRevC.99.044305

I. INTRODUCTION

The phenomenon of superdeformation was used many years ago to explain the fission isomers observed in the actinide nuclei [1]. The curiosity for the superdeformation phenomena increased exponentially when a superdeformed (SD) band in the ^{152}Dy nucleus was observed [2]. Many surprising properties of SD nuclei were observed experimentally, such as constant energy spacing between the transitions, lack of the transition linking the yrast SD band to the normal deformed (ND) states resulting in the $1-2\hbar$ uncertainty in the spin assignments of the SD bands, etc. The nucleon-configuration assignment of the SD bands is based on the systematic behavior of properties such as dynamic ($\Im^{(2)}$) moment of inertia (MoI) and transition quadrupole moments. In the $A \approx 190$ mass region, SD bands were first observed in ^{191}Hg and to date, many other SD bands have been reported [3,4].

The superdeformation spectroscopy has provided us with a great deal of information concerning the behavior of MoI in the SD nuclei. The kinematic ($\Im^{(1)}$) and dynamic MoI ($\Im^{(2)}$) are two types of MoI explored in the SD nuclei. Since calculation of $\Im^{(1)}$ requires the knowledge of spins, $\Im^{(2)}$ is frequently studied in the SD states. A smooth rise of $\Im^{(2)}$ with increasing rotational frequency ($\hbar\omega$) is observed in the $A \approx 190$ mass region, which is a characteristics feature of the SD bands in this mass region. This smooth rise in $\Im^{(2)}$ with $\hbar\omega$ in $A \approx 190$ mass region is interpreted as the alignment of both high-N quasiprotons and quasineutrons and reduction in pairing [5,6]. The resemblance of the yrast SD band of the ^{192}Hg and ^{194}Pb suggested that additional protons do not change the core properties of the SD bands and it was anticipated that odd-A Pb isotopes might have the same properties to their Hg isotones. However, an appealing feature of the odd-A isotopes in Pb is the observation of $\Im^{(2)}$, which remains nearly constant with the increasing rotational frequency (known as "flat" SD bands). Apart from these nuclei, flat SD bands were also observed in the ^{192}Tl where $\Im^{(2)}$ does not increase with $\hbar\omega$. The Pauli blocking [7] of the intruder quasiproton and quasineutron is accountable for the decreased slope of $\Im^{(2)}$. This mass region is also known for the vast majority of observations of the identical SD bands [8–10].

Very recently, the ground-state energy E_2^+ has been split into the shape fluctuation and rotational energy using the shape fluctuation model (SF model). Its variation with the asymmetry parameter γ_0 has been explored to study the structural anomalies in nuclear structure [11]. In this paper, we have systematically studied the flat SD bands available in the Tl and Pb isotopes using the shape fluctuation model (SF model), vibrational distortion model, nuclear softness (NS) formula, semiclassical particle rotor model (PRM), and exponential model with pairing attenuation.

II. ROTATIONAL ENERGY FORMULAE

A. Shape fluctuation model

The shape fluctuation model (SF model) [12] provided a good measure to calculate the variation of the intrinsic shape in the ground-state band. The energy expression of the SF model is given as

$$\begin{aligned} E(I) &= E_0 + E'\phi'I + (B_0 + \phi'B')I(I+1), \\ &= B_0 I(I+1) + E'\phi'I + \phi'B'I^2(I+1), \end{aligned} \tag{1}$$

where E and B are the Hartree-Fock energy and inverse of twice of the moment of inertia (MoI), respectively. In Eq. (1), the first term is the energy due to the rotation of the unfluctuated core, called rotational energy (E_γ^{ROT}). The second and third terms give the excess in the intrinsic energy and the rotational energy due to the fluctuation of the core. The

*dadwal.anshul@gmail.com

second term corresponds to the phonon spectrum while the third term gives the rotational spectrum characterized by a spin-dependent inverse of MoI-like factor. The contribution from these two terms is referred to the shape fluctuation energy ($E_\gamma^{\rm SF}$).

B. Semiclassical vibration distortion model

Using the effect analogous to the vibration and rotation of the nuclei and molecules, the vibrational distortion model was proposed [13]. The energy of excitation in the case of molecules with a rotational and vibrational degree of freedom can be expressed as

$$F_\nu = (B_\nu - D_\nu I(I+1))I(I+1), \tag{2}$$

where ν is the vibrational frequency. Using this expression, the moment of inertia can be expressed as the function of rotational and vibrational distortion as

$$\Im^{(2)} = \Im_c^{(2)} \pm \Im_{\rm vib}^{(2)}[\omega_{\rm max} - \omega/\omega_{\rm max}]^2, \tag{3}$$

where $\Im_c^{(2)}$ and $\Im_{\rm vib}^{(2)}$ are the constant and vibration part of the dynamic MoI, respectively

C. NS formula

The energy levels of ground-state bands in even-even nuclei [14], well-deformed, and transitional nuclei [15] have been described efficiently with the nuclear softness (NS) formula

$$E_I = \frac{\hbar^2 I(I+1)}{2\Im_0}\frac{1}{(1+\sigma_1 I)} \times\left(1 - \frac{\sigma_2 I^2}{(1+\sigma_1 I+\sigma_2 I^2)} - \frac{\sigma_3 I^3}{(1+\sigma_1 I+\sigma_3 I^3)} + \cdots\right), \tag{4}$$

where,

$$\sigma_1 = \frac{1}{\Im_0}\frac{\Delta\Im_0}{\Delta I}, \quad \sigma_2 = \frac{1}{2!\Im_0}\frac{\partial^2\Im_0}{\partial I^2}, \quad \sigma_3 = \frac{1}{3!\Im_0}\frac{\partial^3\Im_0}{\partial I^3}\ldots, \tag{5}$$

are the constants of first, second, third, etc. order of the nuclear softness. Keeping the nuclear softness to only first order, i.e., putting $\sigma_2, \sigma_3 \ldots = 0$, we get a two-parameter formula (NS2)

$$E(I) = \frac{\hbar^2}{2\Im_0} \times \frac{I(I+1)}{(1+\sigma_1 I)}. \tag{6}$$

D. Semiclassical particle rotor model

In the semiclassical PRM, the axially symmetric Hamiltonian for the rotor plus one valence particle is [16]

$$H = Qj_3^2 + A(I-j)^2.$$

Here total angular momentum I is the sum of the core rotational angular momentum R and the angular momentum of the valence particle j. The rotor energy formula obtained is [17]

$$E(I) = \frac{\hbar^2}{2\Im_{\rm (PRM)}}[I(I+1) - 2iI + i(i+1)], \tag{7}$$

where $\Im_{\rm (PRM)}$ (the average value of moment of inertia over the whole band) and i (the average alignment over a limited range of angular momentum) are the fitting parameters.

E. Exponential model with pairing attenuation

The phenomenological studies of Draper [18] and statistical study of Moretto [19] revealed the dependence of the pairing gap (Δ) on the spin

$$\Delta(I) = \Delta_0\left(1 - \frac{I}{I_c}\right)^{\frac{1}{\nu}}. \tag{8}$$

Taking $\nu = 2$ $I_c = 18\hbar$, Sood and Jain [20] gave a rotational energy expression

$$E(I) = \frac{\hbar^2}{2\Im_{\rm (EXPO)}} I(I+1)e^{\Delta_0\sqrt{1-\frac{I}{I_c}}}, \tag{9}$$

where $\Im_{\rm (EXPO)}$ and Δ_0 are free parameters. The exponential model was also tested in the SD $A \approx 190$ mass region where dynamic MoI increases gradually with rotational spin [21].

III. RESULTS AND DISCUSSION

In the present paper, the flat SD bands of the $A \approx 190$ mass region in Tl and Pb isotopes are systematically explored. This is the first time the flat SD bands of the $A \approx 190$ mass region have been investigated using different rotational energy formulas. The observed γ-transition energies [22] of the SD rotational bands of Tl and Pb isotopes have been least-squares fitted. This approach profits from the comparison of calculated and experimental transition energies and is known as the best-fit method (BFM). The root-mean-square (RMS) deviation

$$\chi = \left[\frac{1}{n}\sum_{n=1}^{n}\left(\frac{E_\gamma^{\rm cal}(I_i) - E_\gamma^{\rm exp}(I_i)}{E_\gamma^{\rm exp}(I_i)}\right)^2\right]^{1/2}, \tag{10}$$

(where n is the number of transitions involved in the fitting) between the calculated and experimental transitions energies is minimum at correct band-head spin assigned to the SD band. First, the band-head spins assignment is crucial for the systematic study of the SD bands. For this purpose, we have used the exponential model with pairing attenuation and further supported our assignment with the help of the NS formula. The band-head spins deduced are discussed in Sec. III A. In Sec. III B, the intraband-γ transition energy of the flat SD bands have been spilt into the rotational energy and shape fluctuation energy part. The role of the vibrational distortion factor and nuclear softness parameter has been discussed in Secs. III C and III D, respectively. The alignments of the flat SD bands and the role of pairing have been discussed in Secs. III E and III F.

A. Band-head spins of the flat SD bands

The intraband γ-transition energies of the flat SD bands ^{193}Pb(1, 2, 9), ^{195}Pb(1, 2), ^{197}Pb(1, 2, 3, 4) of Pb isotopes in the $A \approx 190$ mass region, indexed in the table of SD bands [3] and continuously updated ENSDF database [22], have been fitted to the exponential model [Eq. (9)]. Using a least-squares fitting procedure, the parameters $\Im_{\rm (EXPO)}$, Δ_0 are obtained. It is worthwhile to mention that the parameter $\Im_{\rm (EXPO)}$, Δ_0

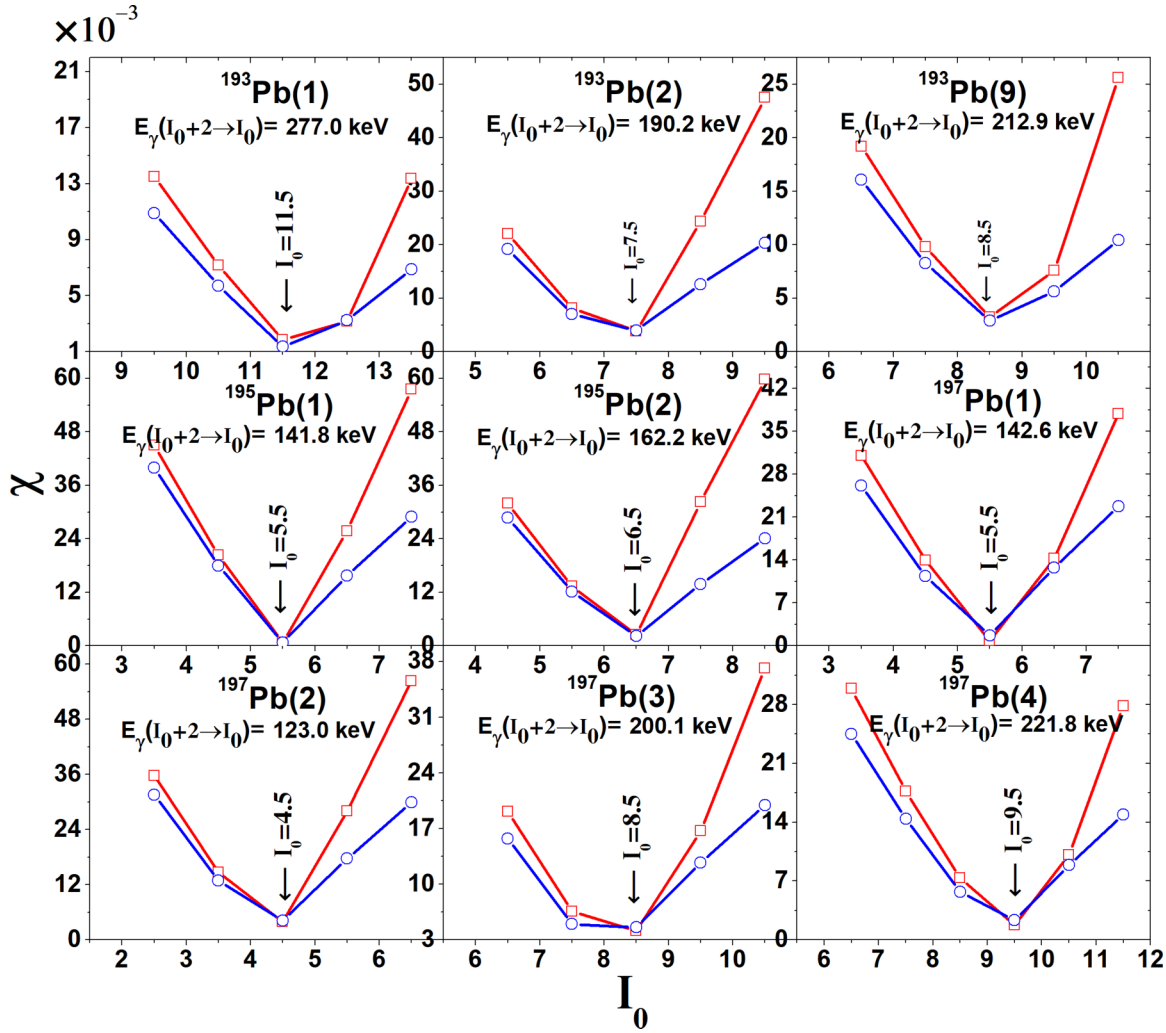

FIG. 1. The RMS deviation plot at various spin assignments for the flat bands ^{193}Pb(1, 2, 9), ^{195}Pb(1, 2), and ^{197}Pb(1, 2, 3, 4) using the exponential model and NS formula. I_0 correspond to the spin value of the lowest level observed. The circles/squares correspond to the values obtained from the NS formula/exponential model.

depends explicitly on the proposed band-head spin. To firmly establish the band-head spins of these nine flat SD bands we have employed the exponential model and further confirmed the spins obtained using the nuclear softness (NS) formula [23]. It is encouraging to mention that, for the flat bands considered here, the band-head spin deduced using the exponential model and NS formula agrees with the previously assigned spin [22], except for ^{193}Pb(2) and ^{195}Pb(1, 2) where band-head spin assigned is $1\hbar$ and $2\hbar$, respectively, lower than the previously assigned spin (see Table II and Fig. 1). For SD band ^{193}Pb(2), the spin fit method is probably inappropriate [24], hence to check the band-head spin assigned for ^{193}Pb(2) we have also employed the ratio-R method [25,26], which provides additional support to the spin assignment. In the ratio-R method, the relation between the kinematic $\Im^{(1)}$ and dynamic $\Im^{(2)}$ MoI is analyzed in the framework of two parameter *ab* formula, $E(I) = a[\sqrt{1 + bI(I+1)} - 1]$ [25,26]. According to the *ab* formula for rotational spectrum, the ratio-R $\equiv \sqrt{[\Im^{(1)}]^3/\Im^{(2)}}$ should be spin independent. Using ratio-R method, the obtained $I_0 = 7.5$ for ^{193}Pb(2) SD band is in accordance with the exponential model and NS formula. Using a less precise analysis of the quasicontinuum component of decay [27], the band-head spins of ^{195}Pb(1) and ^{195}Pb(2) were estimated to be 7.5 and 8.5, respectively. Using the exponential model and NS formula, we find that the band-head spins of ^{195}Pb(1) and ^{195}Pb(2) are 5.5 and 6.5, respectively (see Table II). This is not only in agreement with the previous spin assignment by Farris *et al.* [28] but also coincides with the other theoretical model [29]. As an illustrative example, we have shown the χ vs. I_0 plot for the flat SD bands in Fig. 1 and Table II comprises the band-head spins and parameters of all the SD bands available in odd-A Pb isotopes deduced from the exponential model/NS formula. The band-head spins and parameters of the Tl isotopes have been taken from the Ref. [23].

B. Shape fluctuation energy of the flat SD bands

Using the accurate band-head spins and the intraband γ-transition energies [3,22] of SD bands in Tl and Pb isotopes

TABLE I. Parameters obtained from the least-squares fitting for the SD bands in Tl and Pb isotopes using the SF model. I_0 corresponds to the band-head spin taken from Refs. [22,23] and $\Im$ is the MoI. The RMS deviation is $\chi \times 10^{-3}$.

Band	I_0 ($\hbar$)	E_γ (keV)	B_0 (keV)	$\Im = 1/2B_0$ ($\hbar^2$keV^{-1})	$B'\phi'$ (keV)	$E'\phi'$ (keV)	χ
^{189}Tl(1)	14.5	367.9	6.0444	0.0827	− 0.01798	3.9221	5.1
^{189}Tl(2)	13.5	344.8	6.1686	0.0811	− 0.02061	0.7758	1.2
^{191}Tl(1)	9.5	276.5	5.8859	0.0849	− 0.01816	14.9234	0.7
^{191}Tl(2)	10.5	296.3	5.9697	0.0838	− 0.02052	13.3183	0.7
^{192}Tl(1)	13	283.0	4.8681	0.1027	− 0.00023	− 0.0198	1.4
^{192}Tl(2)	16	337.5	4.9129	0.1018	− 0.00225	− 1.4393	0.7
^{192}Tl(3)	10	233.4	5.3483	0.0935	− 0.01041	− 1.9756	1.3
^{192}Tl(4)	9	213.4	5.4011	0.0926	− 0.01119	− 3.0771	0.5
^{193}Tl(1)	8.5	206.6	5.5719	0.0897	− 0.01388	− 4.0866	0.9
^{193}Tl(2)	9.5	227.3	5.4524	0.0917	− 0.01090	− 2.2444	1.1
^{193}Tl(3)	6.5	187.9	6.1140	0.0818	− 0.02149	− 1.1393	5.4
^{193}Tl(4)	10.5	250.8	5.3105	0.0942	− 0.00816	2.3727	4.4
^{193}Tl(5)	10.5	271.5	5.6301	0.0888	− 0.01389	7.0016	1.5
^{194}Tl(1)	12	271.5	5.6927	0.0878	− 0.01389	− 10.0034	1.5
^{194}Tl(2)	9	209.3	5.2834	0.0946	− 0.00996	− 3.2649	0.6
^{194}Tl(3)	10	240.5	5.5236	0.0905	− 0.01255	− 2.5228	1.8
^{194}Tl(4)	9	220.3	5.4144	0.0923	− 0.01093	− 0.3673	1.3
^{194}Tl(5)	8	187.9	4.9896	0.1002	− 0.00628	0.7436	0.6
^{194}Tl(6)	9	207.0	4.9994	0.1000	− 0.00584	0.3777	1.2
^{195}Tl(1)	5.5	146.2	5.6361	0.0887	− 0.01379	− 4.4227	2.5
^{195}Tl(2)	6.5	167.5	5.7265	0.0873	− 0.01665	− 5.4983	2.6
^{192}Pb(1)	8	214.8	6.0527	0.0826	− 0.02071	− 0.9820	4.1
^{193}Pb(1)	11.5	277.0	5.3642	0.0932	− 0.00627	1.8472	0.9
^{193}Pb(2)	7.5	190.2	5.6143	0.0891	− 0.00624	− 4.9477	1.9
^{193}Pb(3)	10.5	251.5	5.4836	0.0912	− 0.01012	− 1.6748	0.9
^{193}Pb(4)	11.5	273.0	5.7032	0.0877	− 0.01568	− 4.0720	0.8
^{193}Pb(5)	8.5	213.2	5.5898	0.0894	− 0.01335	− 1.0632	1.4
^{193}Pb(6)	9.5	234.6	5.5367	0.0903	− 0.01257	0.1380	0.8
^{193}Pb(7)	10.5	260.6	5.5438	0.0902	− 0.01399	3.0812	1.1
^{193}Pb(8)	11.5	281.8	5.4705	0.0914	− 0.01351	5.6123	1.0
^{193}Pb(9)	8.5	212.9	5.2230	0.0957	− 0.00385	3.8141	0.3
^{194}Pb(1)	6	169.5	5.8613	0.0853	− 0.01683	− 0.1349	1.5
^{195}Pb(1)	5.5	141.8	5.1048	0.0979	− 0.00358	− 0.0358	0.7
^{195}Pb(2)	6. 5	162.2	5.1936	0.0963	− 0.00159	− 2.0499	1.5
^{195}Pb(3)	7.5	198.2	5.5019	0.0909	− 0.01236	2.1021	2.9
^{195}Pb(4)	8.5	213.6	5.8190	0.0859	− 0.01700	− 4.2887	2.1
^{196}Pb(1)	6	171.4	6.2294	0.0803	− 0.02038	− 5.3370	3.2
^{196}Pb(2)	8	204.5	5.7180	0.0874	− 0.01464	− 2.1231	1.6
^{196}Pb(3)	9	226.7	5.7086	0.0876	− 0.01469	− 2.1186	1.1
^{197}Pb(1)	7.5	183.7	5.2383	0.0955	− 0.00526	− 1.4532	0.8
^{197}Pb(2)	6.5	163.7	5.3441	0.0936	− 0.00408	− 3.6850	2.9
^{197}Pb(3)	8.5	200.1	5.3789	0.0930	− 0.00757	− 5.5584	0.9
^{197}Pb(4)	9.5	221.8	5.2906	0.0945	− 0.00681	− 3.3542	1.1
^{197}Pb(5)	8.5	237.5	6.2061	0.0806	− 0.02050	− 0.4261	3.1
^{197}Pb(6)	7.5	215.8	6.1463	0.0813	− 0.01954	1.2196	3.0

and employing the BFM; we have calculated the fitting parameters of SF model. The band-head spins assigned and the parameters obtained using the least-squares fitting procedure are shown in Table I. It is important to mention that the RMS deviation between the calculated and experimental transition energies is of the order of 10^{-3}.

Using the parameters obtained from the BFM, we have split the intraband-γ transition energies of the SD bands in the Tl and Pb isotopes into the rotational energy ($E_\gamma^{\rm ROT}$) and shape fluctuation energy ($E_\gamma^{\rm SF}$) and its variation with the increasing rotational frequency is explored. The analysis of the $E_\gamma^{\rm ROT}$ and $E_\gamma^{\rm SF}$ of the Tl isotopes reveals some interesting results. We have noticed that the $E_\gamma^{\rm ROT}$ of all the SD bands in the Tl isotopes increases monotonically with the rotational frequency $\hbar\omega$ (see Fig. 2). In Fig. 2, we have compared the

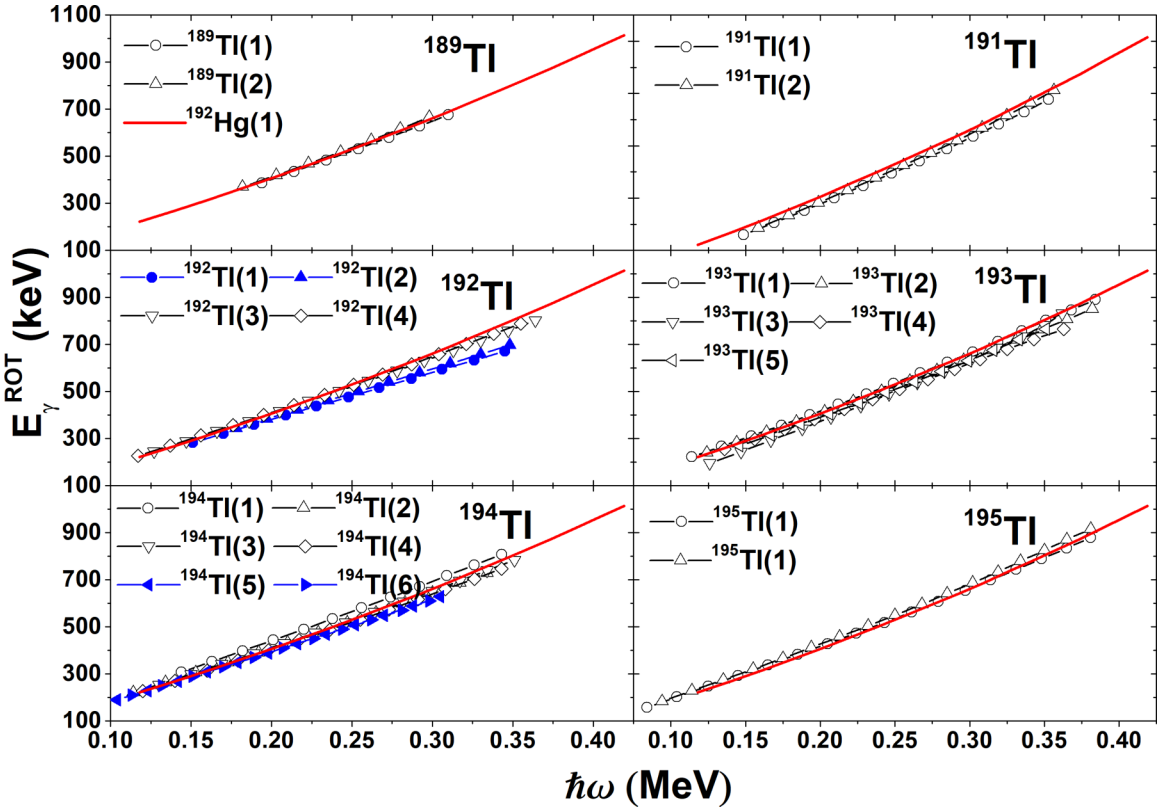

FIG. 2. The variation of the shape fluctuation energy ($E_\gamma^{\rm ROT}$) for SD bands in the Tl isotopes.

$E_\gamma^{\rm ROT}$ of the SD bands in the Tl isotopes with the yrast SD bands in the ^{192}Hg, which have double shell closure at the $Z = 80$ and $N = 112$. It is evident from Fig. 3 that $E_\gamma^{\rm ROT}$ of all the SD bands in Tl isotopes closely follow $E_\gamma^{\rm ROT}$ of the yrast SD band ^{192}Hg(1), except for ^{192}Tl(1, 2) and ^{194}Tl(5, 6). The $E_\gamma^{\rm ROT}$ of ^{192}Tl(1, 2) and ^{194}Tl(5, 6) only follow the ^{192}Hg(1) SD bands curve up to $\hbar\omega \approx 0.20$ MeV. Above $\hbar\omega \approx 0.20$ MeV, the $E_\gamma^{\rm ROT}$ of ^{192}Tl(1, 2) and ^{194}Tl(5, 6) started to split and follow a different curve. This splitting behavior of the $E_\gamma^{\rm ROT}$ is somewhat more distinct in the ^{192}Tl(1, 2) SD bands.

The analysis of $E_\gamma^{\rm SF}$ for all the SD bands of Tl isotopes reveals that $E_\gamma^{\rm SF}$ monotonically decreases with the increasing $\hbar\omega$ (Fig. 3). Also, $E_\gamma^{\rm SF}$ of all the SD bands have a negative value throughout the rotational frequency, except for the ^{191}Tl(1, 2) and ^{193}Tl(5) SD bands, which have positive values at the lowest rotational frequency. The negative sign in $E_\gamma^{\rm SF}$ represents the deexcitation of the core while undergoing fluctuation and its absolute value represents the measure of shape variation in the nuclei [12]. For SD bands ^{191}Tl(1, 2) and ^{193}Tl(5), the small positive values at lowest rotational frequency reflects change in the intrinsic structure as the rotational frequency increases. We have also compared $E_\gamma^{\rm SF}$ of the SD bands in the Tl isotopes with yrast SD band ^{192}Hg(1). Here it is pointed out that all SD bands of the Tl isotopes follow strongly decreasing $E_\gamma^{\rm SF}$ curve of the ^{192}Hg(1) SD band, except for the ^{192}Tl(1, 2) and ^{194}Tl(5, 6). It is quite evident from Fig. 3 that $E_\gamma^{\rm SF}$ of ^{192}Tl(1, 2) SD bands do not vary at all with the increasing frequency and remain constant throughout. Further, it is interesting to note that $E_\gamma^{\rm SF}$ of ^{192}Tl(1, 2) SD bands remain close to ≈0 keV. For all other SD bands of the Tl isotopes, $E_\gamma^{\rm SF}$ varies drastically with the increasing $\hbar\omega$. A similar trend is also evident for the SD bands ^{194}Tl(5, 6), where $E_\gamma^{\rm SF}$ has minimal contribution to the intraband transition energies.

Just as we have split the intraband γ-transition energies of the SD bands in the Tl isotopes, similarly, we have split the intraband γ-transition energies of the SD bands in the Pb isotopes into $E_\gamma^{\rm ROT}$ and $E_\gamma^{\rm SF}$. The results are compared with the yrast SD band in ^{196}Pb (see Figs. 4 and 5). The $E_\gamma^{\rm ROT}$ variation of the odd-A isotopes of Pb have been shown in Fig. 4. It is evident from the figure that $E_\gamma^{\rm ROT}$ of all the SD bands in Pb isotopes follow $E_\gamma^{\rm ROT}$ curve of ^{196}Pb(1) SD band, except for ^{193}Pb(1, 2, 9), ^{195}Pb(1, 2), and ^{197}Pb(1–4). For these specific bands, the $E_\gamma^{\rm ROT}$ follows the curve of ^{196}Pb(1) SD band only up to ≈0.2 MeV and started splitting after $\hbar\omega \approx 0.3$ MeV (however the splitting is not very large).

The variation of $E_\gamma^{\rm SF}$ with increasing $\hbar\omega$ reveals intriguing results. Just as in the case of ^{192}Tl(1, 2) SD bands, the $E_\gamma^{\rm SF}$ of ^{193}Pb(1, 2, 9), ^{195}Pb(1, 2), and ^{197}Pb(1–4) SD bands do not vary drastically with the increasing $\hbar\omega$. However, other SD bands of the Pb isotopes vary drastically with increasing $\hbar\omega$ and have a large negative contribution of $E_\gamma^{\rm SF}$ to the total

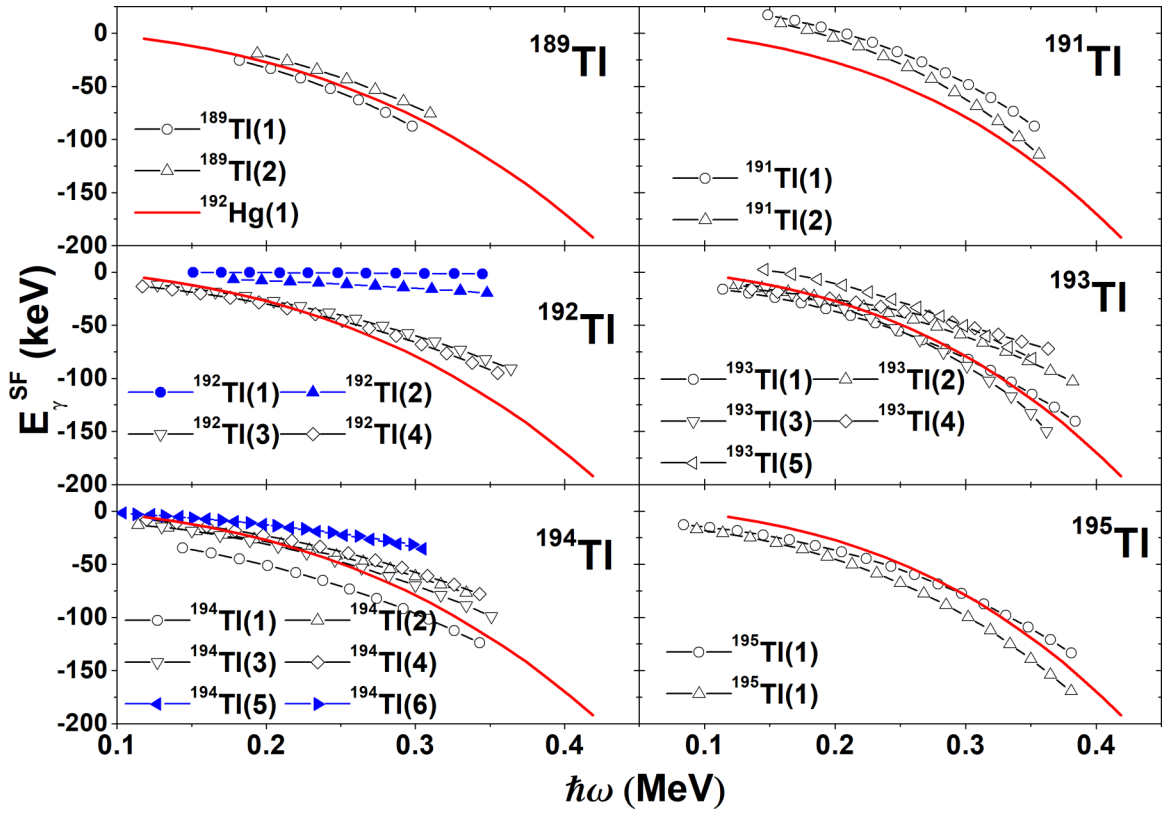

FIG. 3. The variation of the shape fluctuation energy ($E_\gamma^{\rm SF}$) for SD bands in the Tl isotopes.

intraband γ-transitions. It is also evident from Fig. 5 that $E_\gamma^{\rm SF}$ of ^{195}Pb(1, 2) SD bands do not show any variation with the increasing frequency and remain close to ≈0 keV throughout the frequency range.

The fascinating feature of the SD bands ^{192}Tl(1, 2), ^{193}Pb(1, 2, 9), ^{195}Pb(1, 2), and ^{197}Pb(1–4) is that all these SD bands have nearly constant variation of dynamic MoI $\Im^{(2)}$ with increasing rotational frequency and are known as the

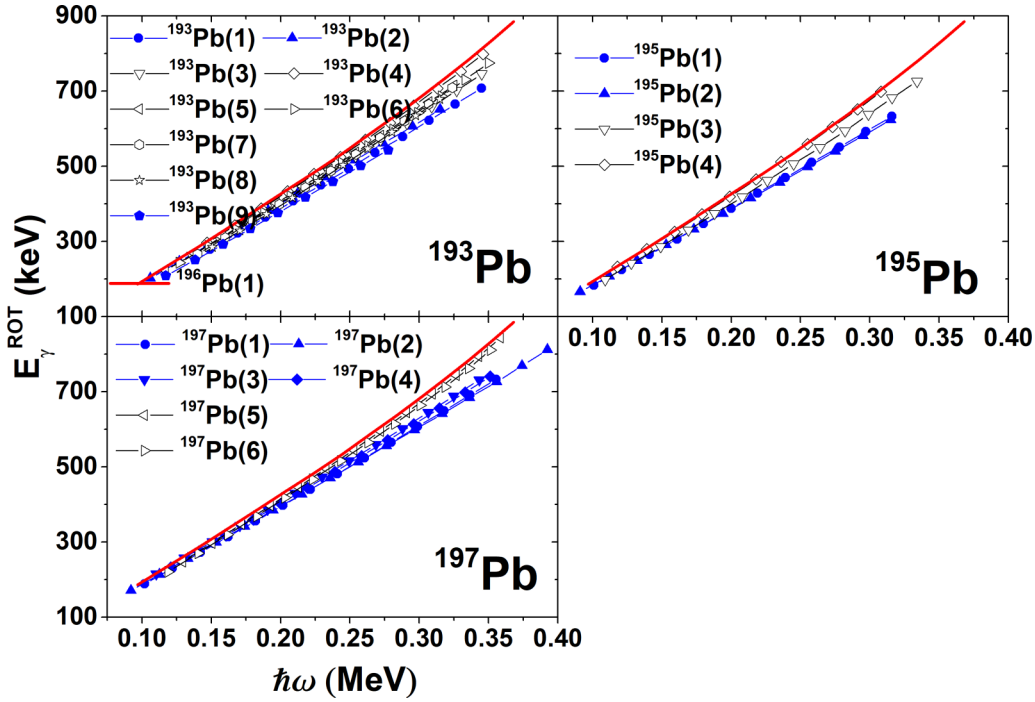

FIG. 4. The variation of the shape fluctuation energy ($E_\gamma^{\rm ROT}$) for SD bands in the Pb isotopes.

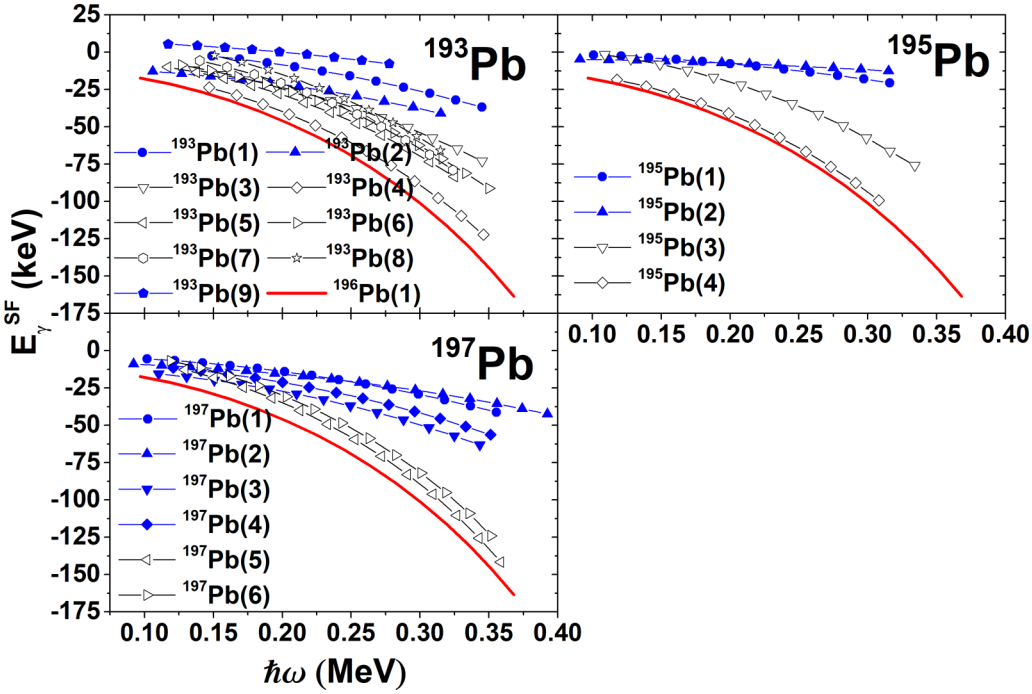

FIG. 5. The variation of the shape fluctuation energy ($E_\gamma^{\rm SF}$) for SD bands in the Pb isotopes.

flat SD bands of the $A \approx 190$ mass region [7,24,28,30–32]. However, the yrast SD bands ^{192}Hg(1) and ^{196}Pb(1) have pronounced increase in the $\Im^{(2)}$ with increasing $\hbar\omega$, which is the characteristic property of the SD bands in the $A \approx 190$ mass region. For SD bands ^{192}Tl(1, 2), the Pauli blocking for quasineutron and proton was proposed to be responsible [7]. However, this cannot be invoked as a valid explanation for the flat bands of the odd-A Pb isotopes. The very small contribution of $E_\gamma^{\rm SF}$ to the total intraband γ transitions reveals that these particular SD bands are insensitive to the shape variation with the increasing $\hbar\omega$.

C. Vibrational distortion factor of the flat SD bands

At this juncture, to support our results we have employed a semiclassical model, which explores the effect of vibrational distortion factor on the MoI as a function of rotational frequency [13]. Here the author has quantified the dynamic MoI as function of rotational frequency and vibration distortion as $\Im^{(2)} = \Im_c^{(2)} \pm \Im_{\rm vib}^{(2)}[\omega_{\rm max} - \omega/\omega_{\rm max}]^2$, where $\Im_c^{(2)}$ and $\Im_{\rm vib}^{(2)}$ are the constant and vibration part of the dynamic MoI, respectively. Using the inputs from this model, we have found that for the SD bands ^{192}Tl(1, 2) and ^{195}Pb(1, 2), the average $\Im_c^{(2)}$ and $\Im_{\rm vib}^{(2)}$ obtained are 103.7 $\hbar^2$MeV^{-1} and 4.3 $\hbar^2$MeV^{-1}. It is interesting to mention here that $\Im_c^{(2)} \approx 110$ $\hbar^2$MeV^{-1} is obtained for all the SD bands in the odd-A Pb isotopes and ^{192}Tl nucleus, however, the coupling of $\Im_{\rm vib}^{(2)}$ is very different, especially for the flat SD bands. For flat SD bands ^{192}Tl(1, 2) and ^{195}Pb(1, 2), $\Im_{\rm vib}^{(2)}$ is negligible ($\approx$4.3 $\hbar^2$MeV^{-1}) when compared with the other SD bands within the same isotope having $\Im_{\rm vib}^{(2)} \approx 59.7$ $\hbar^2$MeV^{-1}. This observation is quite strange for the SD bands in the $A \approx 190$ mass region as it was expected that they might have a higher contribution of the vibrational distortion part [33] than the $A \approx 150$ mass region because of the higher mass. Also, the parameter $\Im_{\rm vib}^{(2)}$ describes the magnitude of deviation from the perfect rigid rotor behavior [13] implying that the smaller the magnitude of $\Im_{\rm vib}^{(2)}$ of the SD band, the closer it is to the perfect rigid rotor. The observation of minimal $\Im_{\rm vib}^{(2)}$ for ^{192}Tl(1, 2) and ^{195}Pb(1, 2) SD bands implies that these SD bands exhibit a perfect rigid rotor behavior. Hence, different magnitude of coupling of the vibrational component is a major reason for the different behavior of dynamic MoI in the flat SD bands. Also, it was proposed that only at the highest rotational frequency, the vibrational distortion should go to zero [33], hence, the negligible $\Im_{\rm vib}^{(2)}$ for the flat SD bands implies that these SD bands are of purely rotational character and any vibrational distortion already becomes zero at lowest rotational frequency. This gives strength to our previous proposition using the SF model where it is calculated that the flat SD bands have minimum shape fluctuations or distortions and maximum rigid core component values.

D. Nuclear softness parameter of the flat SD bands

At this point, we have also calculated the softness parameter of the SD bands in the odd-A Pb isotopes using the nuclear softness (NS) formula [23] to further solidify our proposition of higher deformation in the flat SD bands. The softness parameter (σ) is found to be a good parameter to determine the rigid rotor behavior of the SD bands, i.e., the larger the deformation, the smaller the softness parameter and the higher is the rigidity [34]. We observed that the softness parameter σ obtained is very small for the flat bands when compared with the normal SD bands (SD bands except flat bands, which show a pronounced increase in dynamic MoI)

TABLE II. Parameters obtained using the NS formula and exponential model for 19 SD bands of odd-A Pb isotopes in the $A \approx 190$ mass region. Here 1, 2, 3 . . . in the parenthesis represent band 1, band 2, band 3,. . . , respectively. The SD bands marked by asterisks (∗) represent the flat SD bands. The RMS deviation $\chi(\times 10^{-3})$ is given by Eq. (10).

SD	$E_\gamma^{\exp}$	I_0	NS formula			Exponential model			
bands	$(I_0+2 \rightarrow I_0)$ (keV)	($\hbar$)	$\Im_0$ ($\hbar^2$MeV^{-1})	$\sigma \times 10^{-4}$	χ^{NS}	Δ_0	$\Im_{\rm EXPO}$ ($\hbar^2$MeV^{-1})	$\Im_0'$ ($\hbar^2$MeV^{-1})	$\chi^{\rm EXPO}$
^{193}Pb(1)*	277.0	11.5	91.6	14.9	1.4	0.186	111.3	92.4	1.9
^{193}Pb(2)*	190.2	7.5	93.4	4.0	3.9	0.056	98.9	93.4	3.9
^{193}Pb(3)	251.5	10.5	92.1	19.1	1.7	0.236	117.7	93.0	1.1
^{193}Pb(4)	273.0	11.5	89.5	29.4	2.7	0.347	129.0	91.2	1.1
^{193}Pb(5)	213.2	8.5	89.6	27.0	2.5	0.328	126.2	90.9	1.6
^{193}Pb(6)	234.6	9.5	89.5	27.1	1.3	0.324	125.8	91.0	1.3
^{193}Pb(7)	260.6	10.5	87.0	34.4	1.1	0.412	134.0	88.7	2.5
^{193}Pb(8)	281.8	11.5	86.3	37.0	1.2	0.443	137.1	88.0	2.8
^{193}Pb(9)*	212.9	8.5	91.9	14.8	2.9	0.198	112.6	92.4	3.2
^{195}Pb(1)*	141.8	5.5	97.9	7.3	0.8	0.097	108.2	98.2	0.8
^{195}Pb(2)*	162.2	6.5	98.3	-0.2	2.2	0.000	98.2	98.2	2.4
^{195}Pb(3)	198.2	7.5	88.6	29.3	3.6	0.358	128.6	89.7	4.9
^{195}Pb(4)	213.6	8.5	88.6	28.6	4.5	0.362	128.9	89.8	3.4
^{197}Pb(1)*	142.6	5.5	96.5	9.3	1.7	0.114	108.7	96.9	0.8
^{197}Pb(2)*	123.0	4.5	96.5	3.9	4.2	0.051	101.7	96.6	3.9
^{197}Pb(3)*	200.1	8.5	97.5	8.3	4.6	0.109	109.1	97.8	4.1
^{197}Pb(4)*	221.8	9.5	97.1	10.1	2.3	0.128	111.0	97.6	1.7
^{197}Pb(5)	237.5	8.5	79.6	41.7	3.2	0.486	132.6	81.5	3.4
^{197}Pb(6)	215.8	7.5	79.4	41.6	3.1	0.490	132.8	81.4	4.4

within the same isotope (see Table II). Moreover, we found that the softness parameter is even smaller for the SD bands ^{192}Tl(1) and ^{195}Pb(2), when compared to the other flat SD bands within the same isotope (softness parameter for SD bands in the Tl isotopes have been calculated in Ref. [23]). This observation of negligible softness parameter may imply that the anomalous behavior of the flat SD bands could be because of the higher deformation or superrigid character in these SD bands.

E. Alignment of the flat SD bands

The aligned angular momentum or alignment (i) is one of the most significant quantities, which indicates the nature of the SD bands. The semiclassical particle rotor model (PRM) [16,17] has been effective in deducing the alignments of identical SD bands of the $A \approx 150, 190$ mass region [9,10], where natural/unnatural alignments have been postulated [35]. Motivated by the small contribution of $E_\gamma^{\rm SF}$ and negligible value of the $\Im_{\rm vib}^{(2)}$, σ obtained for the flat SD bands, we have calculated the alignments of SD bands in the Tl and Pb isotopes (see Fig. 6). We have noticed that for flat SD bands available in the Tl [^{192}Tl(1, 2)] and Pb [^{193}Pb(1, 2, 9), ^{195}Pb(1, 2), and ^{197}Pb(1 − 4)] isotopes the alignment obtained is very small when compared with the alignments obtained for other SD bands within same isotope. We have further noticed that the alignment i is particularly zero (≈0.0 $\hbar$) for the SD bands ^{192}Tl(1) and ^{195}Pb(2), however, alignments $i \approx -2.2\ \hbar$ and $i \approx -4.0\ \hbar$ is obtained for the yrast SD bands in ^{196}Pb and ^{192}Hg, respectively. This seems surprising since our calculations using the SF model,

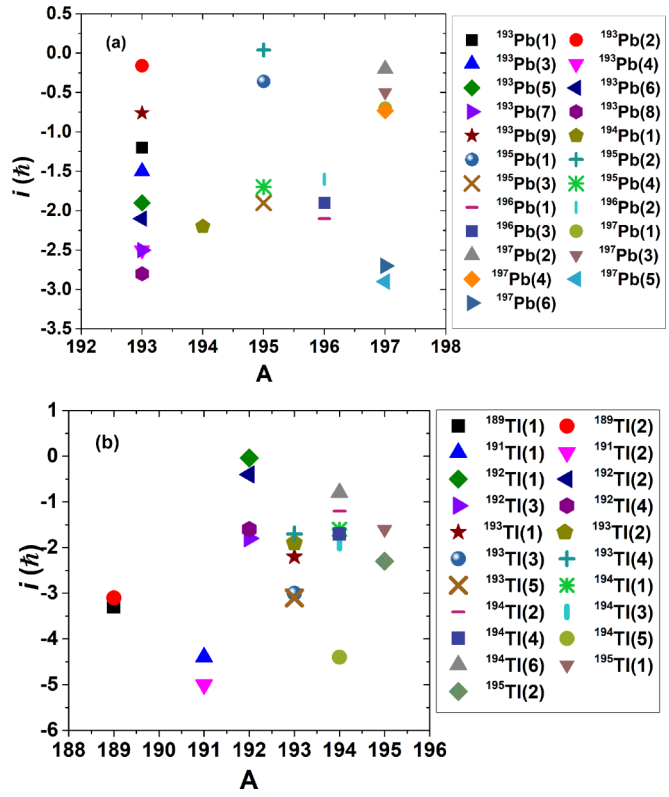

FIG. 6. (a) The fitted values of alignment i obtained from the semiclassical PRM for the SD bands in the Pb isotopes. (b) The fitted values of alignment i obtained from the semiclassical PRM for the SD bands in the Tl isotopes.

vibrational distortion model, and NS formula specifically show that these SD bands have a different behavior of $E_\gamma^{\rm SF}$, $\Im^{(2)}_{\rm vib}$, and σ than the rest of the SD bands in the $A \approx 190$ mass region. For rest of the SD bands (i.e., SD bands except flat bands), we have obtained negative values of alignments in Tl and Pb isotopes. It was proposed that for negative alignments, the involvement of high-j configurations are responsible [17]. In addition, the PRM for single-j configuration based on semiclassical quantization (SCQ) procedure predict a negative value of aligned angular momentum for a considerable range of angular momentum [17]. The negligible alignment obtained for the flat SD bands and almost zero alignment for ^{192}Tl(1) and ^{195}Pb(2) in particular, implies that the high-j configuration in these bands does not show any alignment with the increasing rotational frequency. This result is in accordance with the proposed delayed proton alignment of the flat SD bands [32], which could be due to the enhanced deformation (superrigid character) as calculated from the variation of $E_\gamma^{\rm SF}$ with $\hbar\omega$ and negligible $\Im^{(2)}_{\rm vib}$, σ parameters.

F. Pairing gap parameter of the flat SD bands

The intraband γ-transition energies of the flat SD bands ^{193}Pb(1, 2, 9), ^{195}Pb(1, 2), ^{197}Pb(1, 2, 3, 4) of the Pb isotopes and ^{192}Tl(1, 2) of the Tl isotopes in the $A \approx 190$ mass region have been fitted to the exponential model. The systematic study of these bands on ^{193}Pb using exponential model reveals very surprising results. For flat bands ^{193}Pb(1, 2, 9), the effective pairing parameter Δ_0 is negligible $\approx$0.1–0.2 when compared with other SD bands of ^{193}Pb, which show a continuous increase in the $\Im^{(2)}$ with increasing $\hbar\omega$ (normal SD bands) (see Table II). Initially, in the cranked-shell model (CSM), the pairing interaction was taken to be of monopole type with an initial value of 0.7 MeV at $\hbar\omega = 0$ MeV [24]. Using the exponential model, the effective pairing parameter obtained for flat bands is very small when compared with the CSM value. Also, the frequency dependence of the $\Im^{(2)}$ for favored $N = 7$ band ^{193}Pb(1) was found to be in variance with the similar bands in odd-Hg nuclei (^{191}Hg) [24], which show a substantial rise in $\Im^{(2)}$ with $\hbar\omega$. Since the Δ_0 parameter depends explicitly upon the band-head spin assigned, a definite band-head spin should be assigned to the SD band ^{191}Hg(1). Using the NS formula [23], we assigned $I_0 = 12.5\ \hbar$ to ^{191}Hg(1) SD band. Interestingly, Δ_0 parameter obtained for favored $N = 7$ neutron orbital in the $N = 111$ isotone, ^{191}Hg(1) at $I_0 = 12.5\ \hbar$ ($\Delta_0 = 0.375$), is twice the Δ_0 parameter obtained for similar band in odd-A nucleus, ^{193}Pb(1) ($\Delta_0 = 0.186$). The two times larger Δ_0 parameter obtained for ^{191}Hg(1) than ^{193}Pb(1) could be the reason for different behavior of $\Im^{(2)}$ for the favored $N = 7$ bands. Also, it is found that for the SD bands of the $A \approx 190$ mass region, the configuration-mixing interactions such as pairing are strong enough to reduce the influence of high-N states [36].

Just as ^{193}Pb isotope, the SD bands ^{195}Pb(1, 2) also do not show the rise in $\Im^{(2)}$ with $\hbar\omega$. For flat bands ^{195}Pb(1, 2), the value of Δ_0 is in coincidence with the Δ_0 obtained for the flat bands of ^{193}Pb, where Δ_0 is almost negligible. It is worth noting that for SD band ^{195}Pb(2), Δ_0 is zero. The Δ_0 parameter obtained for the normal SD bands of ^{195}Pb is $\Delta_0 \approx 0.4$, which is four times larger than the Δ_0 parameter obtained for the flat bands (see Table II). Similar four flat bands ^{197}Pb(1, 2, 3, 4) were also observed in ^{197}Pb, however, ^{197}Pb(5, 6) SD bands are the normal SD bands [32,37]. It is evident from Table II that the Δ_0 parameter obtained for flat bands in ^{197}Pb are in accordance with the Δ_0 parameter obtained for the other odd-A isotopes of the Pb ($\Delta_0 \approx 0.1$–0.2). The Δ_0 parameter obtained for the flat bands of ^{197}Pb is $\approx$5–10 times smaller than the Δ_0 parameter of the normal SD bands (see Table II).

Apart from these nuclei of the $A \approx 190$ mass region, the flat bands are also available in ^{192}Tl [7]. Motivated by almost negligible effective pairing parameter obtained for flat bands of the Pb nucleus, we have also calculated the pairing parameter of ^{192}Tl(1, 2). It is very encouraging to mention that using the exponential model for SD bands ^{192}Tl(1) and ^{192}Tl(2), the pairing parameter obtained is 0.006 and 0.043, respectively. These almost negligible values of Δ_0 obtained for the flat bands ^{192}Tl(1, 2) are in coincidence with the values obtained for flat bands of the Pb nucleus.

Since the MoI roughly depends inversely on the pairing correlations, unrealistically large gap parameters were used to include pairing in quasiparticle formulation [5,38]. This reproduces the experimental trend of MoI in Hg nuclei very well where small MoI at low spin is observed [5]. It seems worth mentioning that for the flat bands in ^{195}Pb and ^{197}Pb, the band-head MoI obtained using exponential model is 10–15 $\hbar^2$MeV^{-1} higher when compared with the other SD bands within the same isotope (see Table II). The same systematics of band-head MoI is also true for the flat bands of ^{193}Pb. This observation is in accordance with the inverse dependence of MoI on pairing correlations since pairing correlations obtained using exponential model are almost negligible for flat bands. The flat SD bands of odd-A Pb isotopes, when compared among themselves, reveal that the Δ_0 parameter is even smaller ($\Delta_0 \approx 0.00$–0.06) for flat bands ^{193}Pb(2), ^{195}Pb(2), ^{197}Pb(2), ^{192}Tl(1, 2) (see Table II). Also, the calculation of Δ_0 parameter for the yrast and excited SD bands of the $A \approx 150$, having nearly constant $\Im^{(2)}$ [39], reveal that their Δ_0 parameters ($\Delta_0 \approx 0.01$–0.02) are very similar in magnitude to the Δ_0 parameter obtained for the flat bands ^{193}Pb(2), ^{195}Pb(2), ^{197}Pb(2), ^{192}Tl(1, 2) of the $A \approx 190$ mass region. The negligible Δ_0 parameter obtained for the SD bands of the $A \approx 150$ mass region is because of the fact that at large deformation, ^{152}Dy is a doubly magic nucleus and thus the pairing correlations are strongly quenched for all the SD bands in the neighboring isotopes/isotones of ^{152}Dy nucleus. The negligible Δ_0 parameter obtained for the $A \approx 150$ mass region and flat bands of the $A \approx 190$ mass region implies that the pairing correlations are strongly quenched in both the cases. The comparative study of the $\Im^{(2)}$ for the flat bands in ^{193}Pb, ^{195}Pb, ^{197}Pb, and ^{192}Tl reveals that the rise in $\Im^{(2)}$ with $\hbar\omega$ is strongly quenched only for ^{193}Pb(2), ^{195}Pb(2), ^{197}Pb(2), and ^{192}Tl(1) SD bands when compared with the other flat bands within the same isotope (see Fig. 7). Furthermore, the average values of the $\Im^{(2)}$ for bands ^{193}Pb(2), ^{195}Pb(2), and ^{197}Pb(2) (96.0 $\hbar^2$MeV^{-1}, 98.3 $\hbar^2$MeV^{-1}, and 99.5 $\hbar^2$MeV^{-1}, respectively) are somewhat smaller than the corresponding values for the flat bands in ^{193}Pb, ^{195}Pb, and ^{197}Pb.

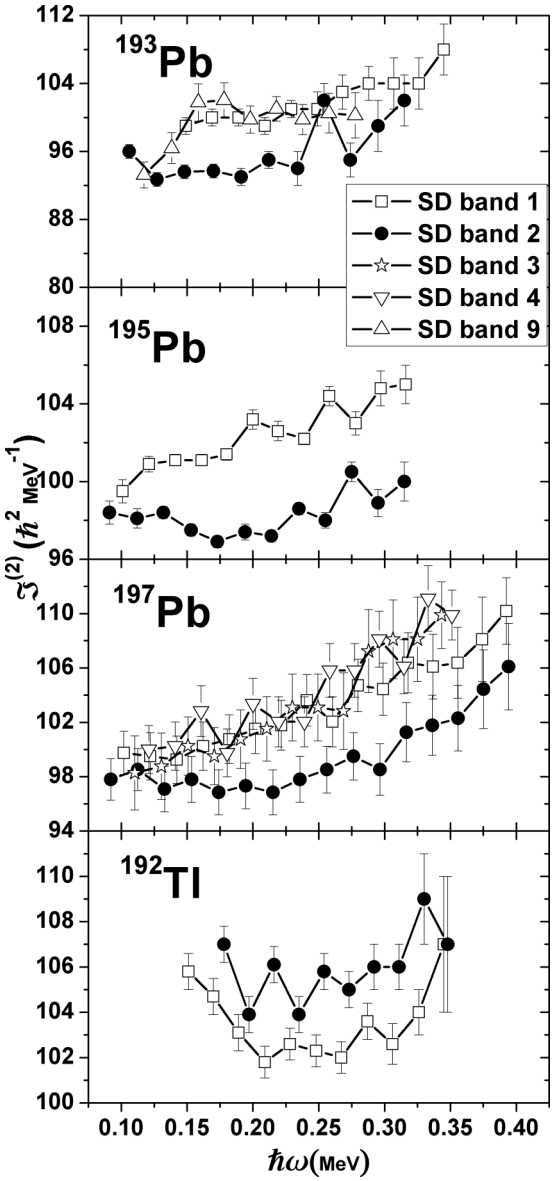

FIG. 7. The variation of experimental dynamic moment of inertia [40] with rotational frequency for flat bands in ^{193}Pb, ^{195}Pb, ^{197}Pb, and ^{192}Tl.

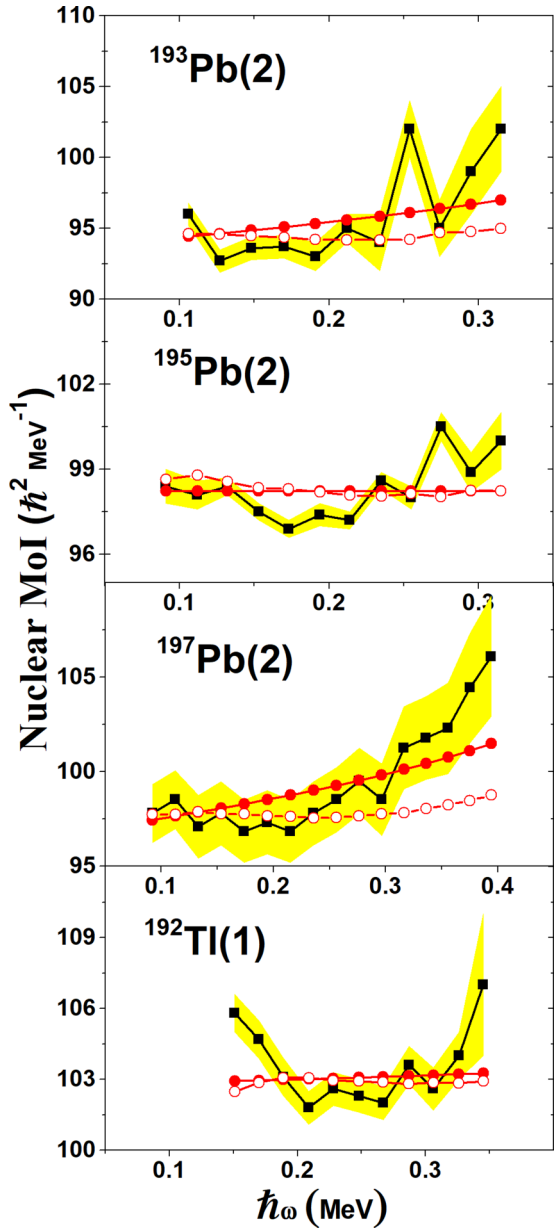

FIG. 8. The variation of calculated kinematic and dynamic moment of inertia with rotational frequency for the flat bands ^{193}Pb(2), ^{195}Pb(2), and ^{197}Pb(2) using the exponential model and comparison with experimental data [40]. The solid/hollow circles correspond to the dynamic/kinematic MoI and solid squares with error (yellow region) correspond to experimental data of dynamic MoI.

It is a well-known fact that for a perfect rigid rotor the kinematic and dynamic MoI should be similar, i.e., $\Im^{(1)} \approx \Im^{(2)}$. Using the deduced band-head spins (see Table II) and calculated transition energies from the exponential model, we have calculated the kinematic and dynamic MoI of the flat SD bands. It is evident from Fig. 8 that the calculated $\Im^{(1)}$ and $\Im^{(2)}$ of flat SD bands ^{193}Pb(2), ^{195}Pb(2), ^{197}Pb(2), and ^{192}Tl(1) are almost identical. Also, the $\Im^{(1)}$ and $\Im^{(2)}$ of flat SD bands ^{195}Pb(2) and ^{192}Tl(1) are identical throughout the observed frequency. This further supports the superrigid character of the flat SD bands, especially of ^{195}Pb(2) and ^{192}Tl(1) bands.

The pairing parameter, Δ_0, is an effective pairing parameter which may include a contribution from the Coriolis antipairing effect as well as from the higher-order cranking effect [21]. Since the static pairing correlation is generally very different for different configurations (e.g., between even and odd nuclei) [41], it was proposed that Δ_0 parameter could be analogous to the dynamic pairing correlation [9]. The almost zero effective pairing parameter obtained for flat bands is consistent with the results of Ref. [5] and Ref. [42], where the dynamic MoI remains constant in no pairing limit. Also, as calculated in Ref. [43], once the pairing correlations disappear, the Hartree-Fock-Bogoliubov (HFB) dynamic MoI becomes identical to the Hartree-Fock (HF) MoI, which remains almost constant with rotational frequency. From this, it can be concluded that the variation in the pairing correlations

is expected to play a substantial role in the SD bands of the $A \approx 190$ mass region.

It is important to mention that $Q_t[^{191}\mathrm{Hg}(1)] \approx Q_t[^{193}\mathrm{Hg}(1)] \approx 17.5eb$ [3], having similar favored $N = 7$ intruder configuration, yet two different variations of dynamic MoI were obtained in both SD bands. Furthermore, similar quadrupole moments $Q_t \approx 20eb$ were obtained for yrast SD bands in ^{194}Pb, ^{196}Pb (normal SD bands) and ^{195}Pb(1, 2) (flat SD bands) [3]. Taking these observations into consideration, it is not necessary that the occupation of high-N states or the enhanced deformation alone is responsible for the flat behavior of dynamic MoI in the Tl and odd-A Pb isotopes. Our proposition is also supported by Ref. [36] where it was concluded that the pairing interactions are sufficient enough to diminish the influence of high-N states in the $A \approx 190$ mass region. Hence, we propose that the neutron intruder orbital blocking and the absence of proton alignment (up to $\hbar\omega \approx 0.35$ MeV) [24] coupled with the negligible value of the pairing correlations [effective pairing parameter Δ_0, which decreases smoothly with spin via. Eq. (9)] could be responsible for the flat bands observed in the $A \approx 190$ mass region.

IV. CONCLUSION

A systematic study of flat SD bands in the Tl and Pb isotopes is made using the shape fluctuation model. The intraband γ-transition energies of the SD bands in the Tl and Pb isotopes have been split into the rotational energy and shape fluctuation part. According to our results, we observe two trends in the SD bands of the Tl and Pb isotopes: (i) SD bands that follow the E_γ^{SF} curve of the yrast SD bands ^{192}Hg and ^{196}Pb and have a pronounced increase in the dynamic MoI with the increasing frequency. (ii) The SD bands that do not follow the E_γ^{SF} curve of the yrast SD bands ^{192}Hg and ^{196}Pb and have nearly constant dynamic MoI with increasing rotational frequency. The SD bands in the classification (ii) [^{192}Tl(1, 2), ^{193}Pb(1, 2, 9), ^{195}Pb(1, 2), and ^{197}Pb(1–4)] follow different E_γ^{SF} curve than the rest of the SD bands in the $A \approx 190$ mass region. The E_γ^{SF} of these curve reveal that they have a negligible contribution to the total intraband γ-transition energies and maximum contribution is from the rotational energy term. The results obtained from the SF model further lend support from the calculation of the minimal vibrational distortion factor $\Im^{(2)}_{\mathrm{vib}}$ for ^{192}Tl(1, 2) and ^{195}Pb(1, 2). The negligible value of the softness parameter and alignments obtained from the NS formula and semiclassical PRM reveals that the deformation is higher and, vice versa, the alignments are negligible for the flat SD bands. The similar systematics of the flat SD bands have been obtained using the exponential model where the effective pairing parameter obtained is negligible.

Taking these evidence into consideration, it seems that the flat SD bands have minimal shape fluctuation energy and effective pairing parameter, and higher deformation. This observation gives support to our proposition that the flat SD bands are superrigid SD bands. Hence, we propose that neutron intruder orbital blocking and the absence of proton alignment (up to $\hbar\omega \approx 0.35$ MeV) coupled with the negligible value of the pairing correlations [effective pairing parameter Δ_0, which decreases smoothly with spin via. Eq. (9)] and larger deformation is responsible for the flat bands observed in the Pb and Tl isotopes. According to the Mottleson-Valatin effect [44], the static pairing is quenched in the SD bands, and any remaining correlations are speculated to be of dynamic character [41]. The observation of almost negligible pairing parameter for the flat bands of the $A \approx 190$ mass region shows that the static and dynamic pairing correlations do not play a significant role for flat bands in the evolution of $\Im^{(2)}$ with increasing $\hbar\omega$.

ACKNOWLEDGMENT

The authors are greatly obliged to Dr. Harleen Dahiya, NIT-J for helpful discussions.

[1] V. M. Strutinsky, Nucl. Phys. A **122**, 1 (1968).
[2] P. J. Twin *et al.*, Phys. Rev. Lett. **57**, 811 (1986).
[3] B. Singh, R. Zywina, and R. B. Firestone, Nucl. Data Sheets **97**, 241 (2002).
[4] E. Ideguchi *et al.*, Phys. Lett. B **686**, 18 (2010).
[5] M. A. Riley *et al.*, Nucl. Phys. A **512**, 178 (1990).
[6] M. W. Drigert *et al.*, Nucl. Phys. A **530**, 452 (1991).
[7] Y. Liang *et al.*, Phys. Rev. C **46**, R2136 (1992).
[8] C. Baktash, B. Haas, and W. Nazarewicz, Annu. Rev. Nucl. Part. Sci. **45**, 485 (1995).
[9] A. Dadwal and H. M. Mittal, Eur. Phys. J. A **53**, 132 (2017).
[10] A. Dadwal and H. M. Mittal, J. Phys. G: Nucl. Part. Phys. **45**, 065103 (2018).
[11] A. Bindra and H. M. Mittal, Nucl. Phys. A **975**, 45 (2018).
[12] M. Sathpathy and L. Sathpathy, Phys. Lett. B **34**, 377 (1971).
[13] S. Roy, Phys. Rev. C **94**, 064329 (2016).
[14] R. K. Gupta, Phys. Lett. B **36**, 173 (1971).
[15] P. von Brentano, N. V. Zamfir, R. F. Casten, W. G. Rellergert, and E. A. McCutchan, Phys. Rev. C **69**, 044314 (2004).
[16] A. K. Jain *et al.*, Phys. Lett. B **392**, 243 (1997).
[17] M. Dudeja *et al.*, Phys. Lett. B **412**, 14 (1997).
[18] J. E. Draper, Phys. Lett. B **41**, 105 (1972).
[19] L. G. Moretto, Nucl. Phys. A **185**, 145 (1972).
[20] P. C. Sood and A. K. Jain, Phys. Rev. C **18**, 1906 (1978).
[21] S.-g. Zhou and C. Zheng, Phys. Rev. C **55**, 2324 (1997).
[22] The ENSDF and XUNDL databases available at http://www.nndc.bnl.gov/chart/
[23] A. Dadwal and H. M. Mittal, Eur. Phys. J. A **53**, 2 (2017).
[24] J. R. Hughes *et al.*, Phys. Rev. C **51**, R447 (1995).
[25] C. S. Wu, L. Cheng, C. Z. Lin, and J. Y. Zeng, Phys. Rev. C **45**, 2507 (1992).
[26] C. S. Wu, J. Y. Zeng, Z. Xing, X. Q. Chen, and J. Meng, Phys. Rev. C **45**, 261 (1992).
[27] M. S. Johnson, J. A. Cizewski, K. Y. Ding, N. Fotiades, M. B. Smith, J. S. Thomas, W. Younes, J. A. Becker, L. A.

Bernstein, K. Hauschild, D. P. McNabb, M. A. Deleplanque, R. M. Diamond, P. Fallon, I. Y. Lee, A. O. Macchiavelli, and F. S. Stephens, Phys. Rev. C **71**, 044310 (2005).
[28] L. P. Farris *et al.*, Phys. Rev. C **51**, R2288 (1995).
[29] S. X. Liu and J. Y. Zeng, Phys. Rev. C **58**, 3266 (1998).
[30] L. Ducroux *et al.*, Phys. Rev. C **53**, 2701 (1996).
[31] D. Robach *et al.*, Nucl. Phys. A **660**, 393 (1999).
[32] I. M. Hibbert *et al.*, Phys. Rev. C **54**, 2253 (1996).
[33] S. Roy, Proc. DAE Symp. on Nucl. Phys. **62**, 302 (2017).
[34] N. Sharma, H. M. Mittal, S. Kumar, and A. K. Jain, Phys. Rev. C **87**, 024322 (2013).
[35] F. S. Stephens *et al.*, Phys. Rev. Lett. **65**, 301 (1990).
[36] G. de France, C. Baktash, B. Haas, and W. Nazarewicz, Phys. Rev. C **53**, R1070(R) (1996).
[37] A. Prevost *et al.*, Eur. Phys. J. A **10**, 13 (2001).
[38] M. P. Carpenter *et al.*, Phys. Lett. B **240**, 44 (1990).
[39] J. K. johansson *et al.*, Phys. Rev. Lett. **63**, 2200 (1989).
[40] X. L. Han and C. L. Wu, At. Data Nucl. Data Tables **73**, 43 (1999).
[41] Y. R. Shimizu, Nucl. Phys. A **520**, 477c (1990).
[42] R. R. Chasman, Phys. Lett. B **242**, 317 (1990).
[43] B. Gall *et al.*, Z. Phys. A **348**, 183 (1994).
[44] B. R. Mottelson and J. D. Valatin, Phys. Rev. Lett. **5**, 511 (1960).